

Vacancy and interstitial oxide ion migration in heavily doped
 $\text{La}_{2-x}\text{Sr}_x\text{CoO}_{4\pm\delta}$ [†]Cristina Tealdi,^{*ab} Chiara Ferrara,^b Piercarlo Mustarelli^b and M. Saiful Islam^c

Received 8th February 2012, Accepted 5th March 2012

DOI: 10.1039/c2jm30769c

$\text{La}_{2-x}\text{Sr}_x\text{CoO}_{4\pm\delta}$, a K_2NiF_4 -type structured oxide, is currently under investigation for its possible application as a cathode material in solid oxide fuel cells operating at intermediate temperature (IT-SOFCs). Here we report a combined energy minimization and molecular dynamics study of oxygen migration mechanisms in the $\text{La}_{2-x}\text{Sr}_x\text{CoO}_{4\pm\delta}$ material for high Sr levels ($x > 0.8$). In the oxygen-deficient composition $\text{La}_{0.8}\text{Sr}_{1.2}\text{CoO}_{3.9}$ the oxide-ion transport mainly occurs through the migration of oxygen vacancies within the perovskite layer of the structure, with possible vacancy paths between adjacent layers. In the oxygen-rich composition $\text{La}_{1.2}\text{Sr}_{0.8}\text{CoO}_{4.1}$ interstitial oxygen transport is *via* an interstitialcy mechanism and within the *ab* plane.

1. Introduction

Layered perovskite oxides belonging to the first member of the Ruddlesden–Popper series ($\text{A}_{n+1}\text{B}_n\text{O}_{3n-1}$; $n = 1$) and exhibiting the K_2NiF_4 -type structure are the subject of considerable interest as they display a variety of physical properties. These cover superconductivity, magnetoresistance, catalysis and mixed ionic–electronic conductivity.¹ The latter, in particular, has attracted recent attention for the possible application of A_2BO_4 compounds (A = rare earth; B = transition metal) as cathode materials in intermediate-temperature solid oxide fuel cells (IT-SOFC).^{2,3} The most extensively studied systems for such applications are Ln_2NiO_4 (Ln = La, Pr, Nd). Both experimental (structural and transport) and modelling studies have focused on oxygen over-stoichiometric compounds,^{4–14} although doping with alkaline-earth atoms on the Ln site can modulate the oxygen content in the system, as well as the average oxidation state of the transition metal ion.¹⁵

Oxygen interstitial migration in La_2NiO_4 -based materials has been shown to be highly anisotropic.¹¹ This is consistent with computer modelling work^{9,11,14} as well as with structural studies based on the maximum entropy method.^{6,7} A recent modelling study on the $\text{La}_2\text{CoO}_{4+\delta}$ compound¹⁴ shows that the oxygen diffusion mechanism is due to a cooperative interstitialcy

mechanism, in agreement with that previously proposed for the related $\text{La}_2\text{NiO}_{4+\delta}$ and $\text{Pr}_2\text{NiO}_{4+\delta}$ systems.¹¹

However, heavily acceptor-doped materials and oxygen diffusion *via* oxygen vacancies have received limited attention; activation energies for oxygen vacancy migration have been calculated for undoped La_2CuO_4 ,¹⁶ and a recent modelling study on undoped La_2NiO_4 based on energy minimization techniques¹³ compares calculated activation energies for vacancy and interstitial migration in this composition.

For the acceptor-doped system $\text{La}_{2-x}\text{Sr}_x\text{CoO}_{4\pm\delta}$, higher total conductivity has been found for the Sr-rich compositions where the Co oxidation state is close to Co^{3+} compared to samples with $x < 1$.^{17,18} This experimental evidence and the suggestion of lower activation energies for oxygen vacancy migration compared to interstitial oxygen in related compounds¹³ are aspects which warrant further consideration in view of potential applications of this class of materials.

In this study, we combine energy minimization and molecular dynamics (MD) techniques to investigate, for the first time, the migration paths and energetics for both oxygen vacancy and interstitial mechanisms in the $\text{La}_{2-x}\text{Sr}_x\text{CoO}_{4\pm\delta}$ system for high Sr levels ($x > 0.8$). Such mechanistic detail is crucial to gain a greater understanding of the transport behavior in K_2NiF_4 -type oxides that underpins their development for next-generation SOFC cathode materials.

2. Methods

In this study, two classes of well established modelling methods have been used, namely static lattice (energy minimization) and molecular dynamics (MD). The GULP code was used for the energy minimization simulations.¹⁹ Interactions between ions were modelled with a Buckingham potential which accounts for electron cloud overlap (Pauli repulsion) and van der Waals

^aINSTM Consortium – Pavia Research Unit, Viale Taramelli 16, 27100 Pavia, Italy. E-mail: cristina.tealdi@unipv.it; Fax: +39 0382 987575; Tel: +39 0382 987569

^bDepartment of Chemistry-Physical Chemistry Division, University of Pavia, Viale Taramelli 16, 27100 Pavia, Italy

^cDepartment of Chemistry, University of Bath, Bath, BA2 7AY UK

[†] Electronic supplementary information (ESI) available: Buckingham potential and shell model parameters; calculated lattice parameters and bond lengths for LaSrCoO_4 in space group 1; examples of mean square displacement (MSD) parameters and fractional atomic coordinates as a function of time. See DOI: 10.1039/c2jm30769c

interactions. Electronic polarizability was treated using the shell model of Dick and Overhauser.²⁰ Lattice relaxation around charged defects was treated using the Mott–Littleton method.²¹

The short-range potential parameters assigned to each ion–ion interaction were derived by empirical fitting to the observed structural properties, starting from established pair-potential parameters. A mean field approach (partial occupancy on the A site) using the space group $I4/mmm$ was initially used for the determination of the suitable potential model and the calculation of basic point defects and activation energies for migration.

Calculations were subsequently performed in the $P1$ group where occupancy equal to 1 has been assigned to La and Sr distinct sites, with the lowest energy configuration used for the subsequent defect calculations. Experimental structural parameters for the LaSrCoO_4 composition were transferred from our previous work.¹⁷ Details of the potential and shell model parameters used in this study are given in Table SI-1 (ESI†).

MD simulations were performed with the DL_POLY code²² using an orthogonal simulation box with periodic boundary conditions. The simulation box consisted of $6 \times 6 \times 4$ unit cells, giving a total of approximately 3000 species in the simulation box; shells were considered for the oxygen atoms only. La and Sr ions, as well as oxygen vacancies and interstitials, were distributed randomly within the simulation box.

Different compositions were reproduced in order to represent both oxygen over-stoichiometric and under-stoichiometric samples. In particular, the following compositions were considered: LaSrCoO_4 , $\text{La}_{0.8}\text{Sr}_{1.2}\text{CoO}_{3.9}$, $\text{La}_{1.2}\text{Sr}_{0.8}\text{CoO}_{4.1}$, $\text{La}_{0.8}\text{Sr}_{1.2}\text{CoO}_{3.95}$, and $\text{La}_{1.2}\text{Sr}_{0.8}\text{CoO}_{4.05}$. In LaSrCoO_4 , no defects are present at the beginning of the simulation and the average oxidation state of Co is 3+, in agreement with the experiment.¹⁵ For the $\text{La}_{0.8}\text{Sr}_{1.2}\text{CoO}_{3.9}$ and $\text{La}_{1.2}\text{Sr}_{0.8}\text{CoO}_{4.1}$ compositions, a totally ionic compensation (oxygen vacancies or interstitials) of the change in the La/Sr ratio was adopted. For the $\text{La}_{0.8}\text{Sr}_{1.2}\text{CoO}_{3.95}$ and $\text{La}_{1.2}\text{Sr}_{0.8}\text{CoO}_{4.05}$ compositions, a partial electronic/ionic compensation of the change in the La/Sr ratio was adopted. In this case, the average Co oxidation state deviates from 3. This last scenario is more representative of the experimental situation. However, since the focus of the present paper is on the mechanistic feature of oxygen transport within this system and, in this respect, we did not notice appreciable differences between the two compensation models proposed, the results presented in the following sections are relative to the totally ionic compensation model. Indeed, for completeness Fig. SI-1 and SI-2† show examples of the most frequent migrating events found for the $\text{La}_{0.8}\text{Sr}_{1.2}\text{CoO}_{3.95}$ and $\text{La}_{1.2}\text{Sr}_{0.8}\text{CoO}_{4.05}$ compositions, indicating the similarity between the totally ionic and partially electronic compensation models in terms of migration mechanisms.

For the MD simulations, the systems were equilibrated first under a constant pressure of 1 atm and at a specific temperature in the range 1373–1973 K for 300 000 time steps (with a time step of 0.5 fs). The average box dimensions derived at each investigated temperature were used during a further equilibration step in the NVT ensemble (Berendsen thermostat) for 60 ps before carrying out the main MD runs of 300 ps. Data analysis was performed using the Visual Molecular Dynamics package (VMD).²³ Such computational techniques have been applied successfully to studies of ion transport in a range of ternary oxides.^{11–14,26–31}

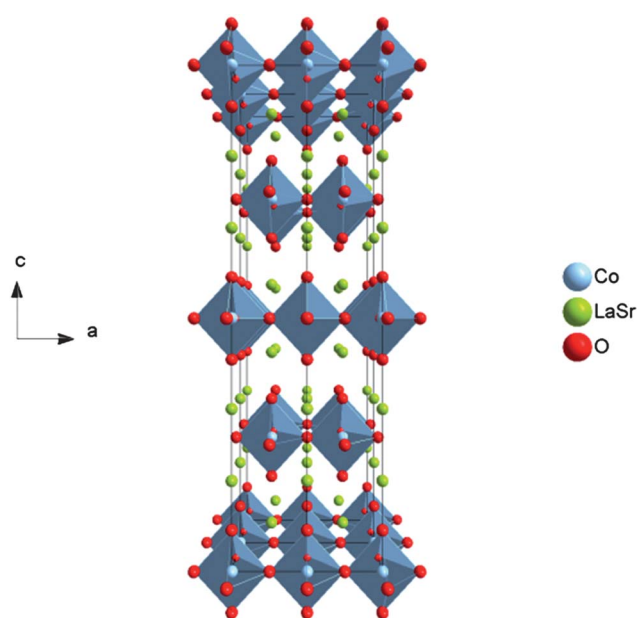


Fig. 1 Perspective view of the LaSrCoO_4 structure showing corner-sharing CoO_6 octahedra and its layered nature.

3. Results and discussion

3.1 Structural modelling and defect sites

LaSrCoO_4 crystallizes in the tetragonal space group $I4/mmm$ (s.g. 139). The structure (Fig. 1) is composed of CoO_6 octahedra connected to form a two-dimensional network by corner-shared oxygen atoms. These layers, similar to those found in the perovskite structure, are separated by (La,Sr)O slabs with the rock-salt structure. Two oxygen crystallographic sites are present within the structure, namely O1 (equatorial position) and O2 (apical position).

First, the potential model succeeded in reproducing the experimental crystal structure, both in the $I4/mmm$ (Table 1) and in the $P1$ (Table SI-2, ESI†) space groups, within 0.1 Å for the lattice parameters and 0.05 Å for the bond lengths. In particular, the CoO_6 octahedral distortion is well reproduced, showing that the elongation of the Co-centred octahedra along the c -axis is preserved. The agreement between experimental and calculated structure forms the basis for the subsequent defect calculations.

Calculations on oxygen defects in the LaSrCoO_4 system indicate a preference for the formation of oxygen vacancies in the equatorial plane, localized on the O1 site of the structure. This is

Table 1 Experimental and calculated lattice parameters and bond lengths for LaSrCoO_4 in space group $I4/mmm$

Parameter	Exp./Å	Calc./Å	$\Delta(\text{exp.} - \text{calc.})/\text{Å}$
a	3.802	3.831	−0.028
c	12.493	12.591	−0.098
La–O2	2.441	2.471	−0.030
La–O1	2.582	2.631	−0.049
La–O2	2.707	2.717	−0.011
Co–O1	1.901	1.915	−0.014
Co–O2	2.059	2.021	0.038

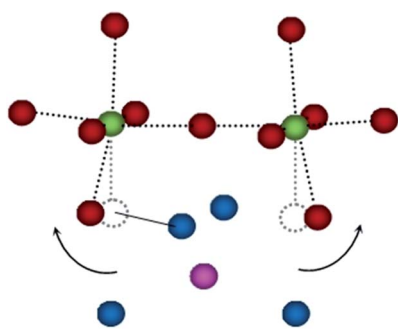


Fig. 2 Schematic representation of the local relaxation around the oxygen interstitial defect. Legend—oxygen interstitial: pink; lattice oxygen: red; Co: green; La/Sr: blue. Grey dotted spheres represent the apical oxygen position before relaxation.

in agreement with previous computational results on related phases, such as the La_2NiO_4 system both in the tetragonal¹³ $I4/mmm$ and the orthorhombic systems.²⁴ The most favorable oxygen interstitial position was found to be (0.50 0.00 0.25), as previously proposed for the La_2NiO_4 system,¹³ and close to the experimentally observed position in Pr_2NiO_4 -based mixed conductors.⁶ Extensive local relaxation occurs around this interstitial position and, as shown in Fig. 2, this consists mainly in the partial tilting of the adjacent CoO_6 octahedra to displace the neighbouring O ions. These results are in accordance with the anisotropic displacement parameters observed from neutron diffraction studies on related structures.⁶

3.2 Oxygen-deficient material: vacancy migration

Several oxygen migration paths and mechanisms have been investigated within the LaSrCoO_4 structure. Static lattice simulations based on energy minimization techniques have been used

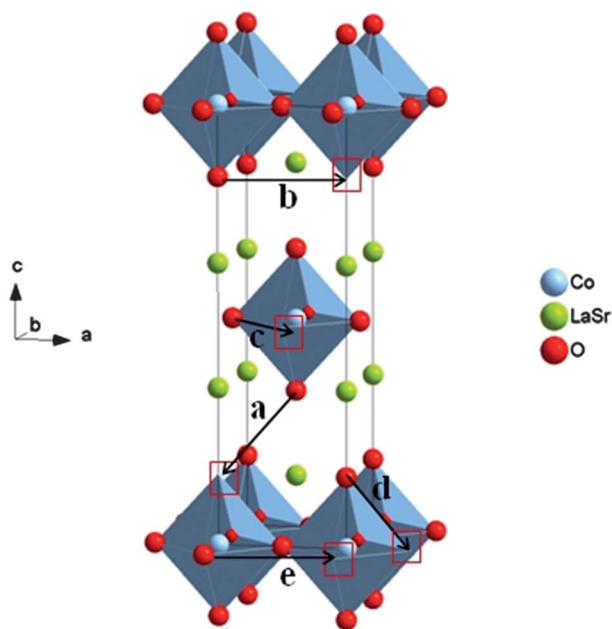


Fig. 3 Schematic representation of the oxygen vacancy migration paths in the LaSrCoO_4 structure.

to calculate the energy profiles for oxygen migration and to derive the activation energy for such processes. These results have been analyzed in view of the scatter plots of atom positions and the trajectory plots from the MD simulations, in order to elucidate the mechanistic features of oxide ion vacancy migration within this system.

Fig. 3 shows schematically the migration paths considered within the unit cell. Oxygen migration *via* vacancy hopping may proceed through one of the paths labelled from a to e. The energy profiles for the ionic migration involved in each of the migration paths presented in Fig. 3 were calculated first considering a linear path between two adjacent equivalent crystallographic positions. Subsequently, possible deviations from the linear path were taken into consideration, allowing the oxygen ion position to relax to the saddle point. This resulted in a curved path characterized by a lower activation energy for migration. Fig. 4 shows a comparison between the linear and curved migration energy profiles related to paths b and c (Fig. 3), selected as examples. It should be noted that, whereas in Fig. 4a (path b of Fig. 3) the difference in activation energy between linear and curved paths is relatively high (approximately 1 eV), in Fig. 4b (path c of Fig. 3) a much smaller difference is found (approximately 0.2 eV).

Table 2 summarizes the calculated activation energies for all the possible migration paths of Fig. 3. These data suggest that the lowest migration energy is for path c, which involves vacancy hopping between two adjacent equatorial (O1) positions within

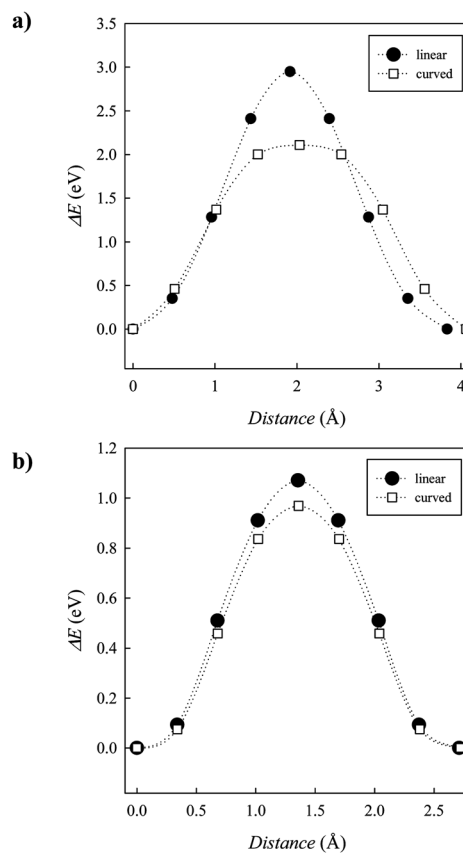


Fig. 4 Energy profile for oxygen vacancy migration *via* linear and curved paths in LaSrCoO_4 : (a) apical–apical position (path b of Fig. 3); (b) equatorial–equatorial position (path c of Fig. 3).

Table 2 Activation energies for oxygen vacancy migration with reference to paths in Fig. 3

Migration path	E_{act} (eV)
a (O2–O2)	1.26
b (O2–O2)	2.11
c (O1–O1)	0.97
d (O2–O1)	1.14
e (O1–O1)	6.02

the ab plane (*i.e.*, the perovskite layer) and along the edge of a CoO_6 octahedron (Fig. 3). As found for ABO_3 perovskites such as NdCoO_3 ,^{26,27} this is predicted to be a slightly curved path where the migrating species is moving away from the central Co ion. Oxygen vacancy migration along paths d (equatorial–apical positions within a CoO_6 octahedron) and a (apical–apical positions involving CoO_6 octahedra in two separate perovskite layers) is also found to be relatively favourable, although with higher migration energies than that found for undoped La_2NiO_4 .¹³

To complement these results and to investigate the mechanistic features of oxide ion vacancy migration in LaSrCoO_4 -based materials in more detail, molecular dynamics (MD) simulations were carried out. Such techniques have proven to be well suited to probe transport mechanisms directly (especially complex correlated ion motion^{28,29}), thus adding to the information derived from the static lattice simulations. Scatter plots of ion coordinates over the simulated time length enable the migration paths to be visualized, and the regions of space most frequently traversed by the different species to be identified. Analysis of the results indicates that oxide ion migration in oxygen-deficient materials proceeds through a vacancy hopping between neighbouring oxygen sites. As expected, no cation diffusion was observed over the simulation time and temperature regime explored.

Fig. 5 shows the scatter plot of ion positions from the MD simulation in a perovskite layer. Fig. 5a shows that no vacancy defects were present at the beginning of the simulation (LaSrCoO_4 stoichiometry). In this case, over the simulation time all the ions vibrate around their starting equilibrium positions, as expected. In Fig. 5b the data related to the $\text{La}_{0.8}\text{Sr}_{1.2}\text{CoO}_{3.9}$ composition are presented. The overlapping of colors in Fig. 5b indicates that considerable migration has occurred in this layer over the simulation time scale, and that oxide ions originally on crystallographically non-equivalent sites (O1 and O2) have exchanged their positions.

Analysis of the scatter plot of ion positions shows that the most frequent transport event is the migration within the ab plane along the edges of CoO_6 octahedra between equatorial (O1) positions (equivalent to path c of Fig. 3). This is in good agreement with the trend in calculated activation energies presented in Table 2. Long-range migration according to this pathway is highlighted in box X of Fig. 5b. This particular event, involving six equatorial oxygen positions, is shown in a 3D representation in Fig. 6 where a segment of the CoO_6 octahedron is illustrated. Fig. 5b also highlights in box Y the curved nature of a vacancy hopping between two equatorial O1 positions (path c of Fig. 3). As predicted by energy minimization, the difference in

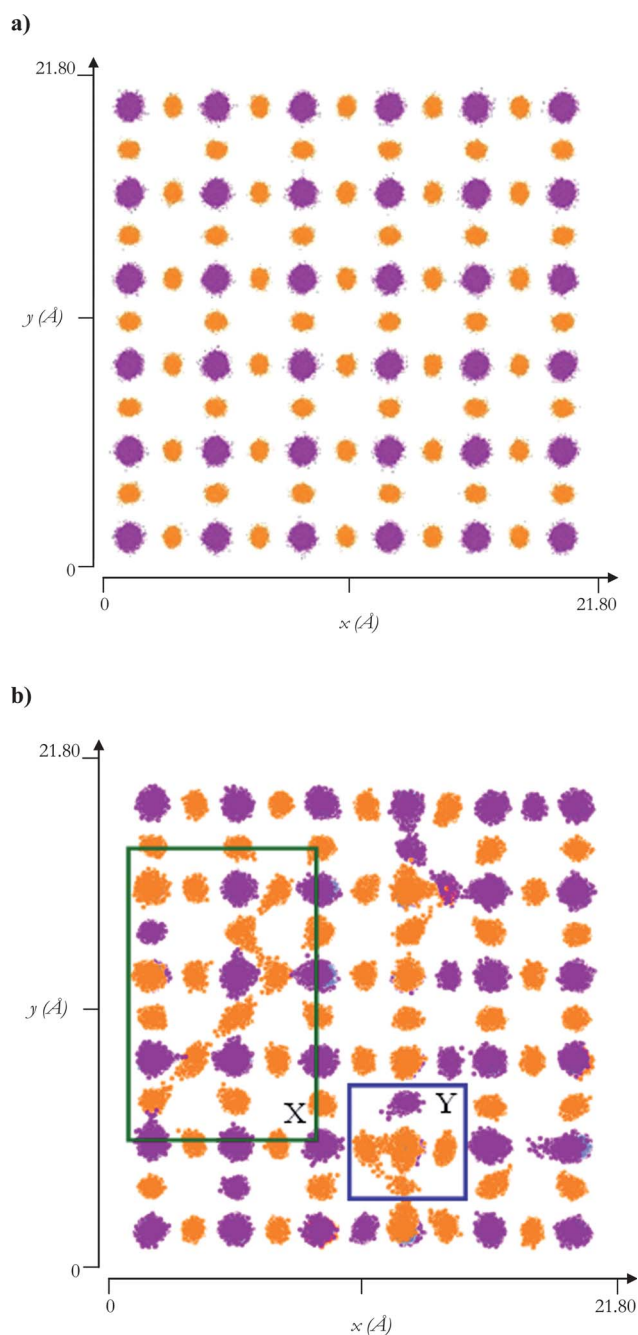


Fig. 5 Scatter plot of ion positions from MD simulations viewed down the c axis of a perovskite layer in (a) LaSrCoO_4 and (b) $\text{La}_{0.8}\text{Sr}_{1.2}\text{CoO}_{3.9}$. Orange, purple and pale blue dots represent ions originally on O1, O2 and Co sites, respectively. La and Sr ions in between layers have been omitted for the sake of clarity.

calculated activation energy between linear and curved paths is in this case relatively small (Fig. 4b). This helps to rationalise our finding that, over the MD simulation time, the migration path is often visualized also as a straight path.

Other frequent migration events found from the analysis of the MD scatter plots of ion positions are presented in Fig. 7, where two adjacent perovskite layers are shown, and indicates vacancy migration associated with paths a and d of Fig. 3. In the first case

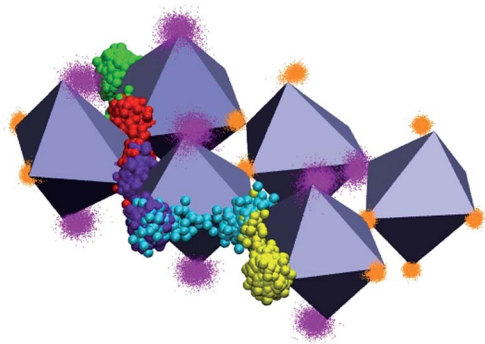


Fig. 6 3D representation of the migration event highlighted in box X of Fig. 5b, showing long-range diffusion involving six equatorial oxygen positions. Each oxygen involved in the migration event is represented by a different colour; spheres of the same colour indicate the positions occupied by a specific atom over the simulation time.

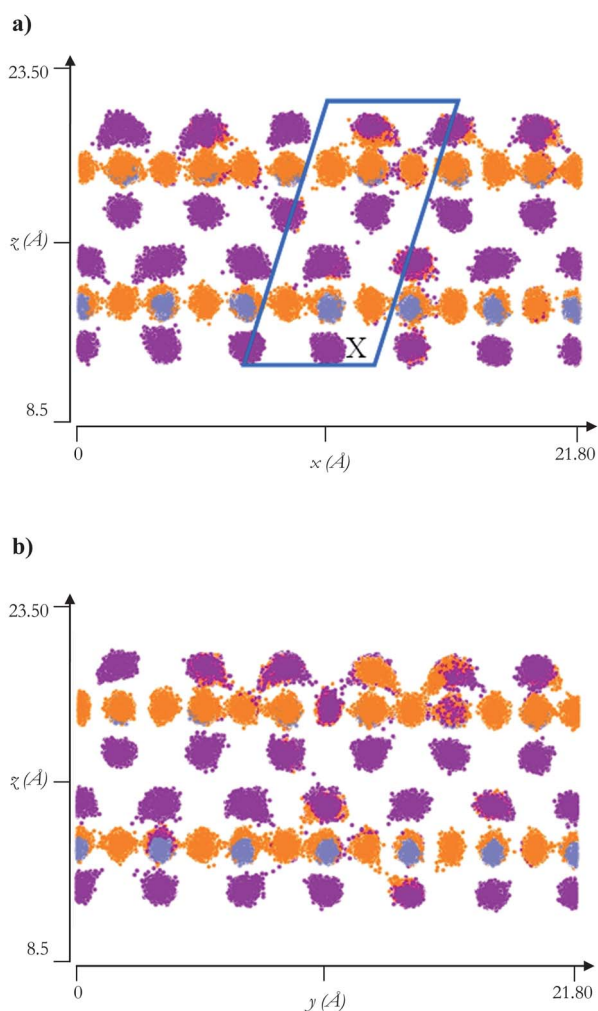


Fig. 7 Scatter plot of ion positions from MD simulations viewed down (a) the *b* axis and (b) the *a* axis for two adjacent perovskite layers in $\text{La}_{0.8}\text{Sr}_{1.2}\text{CoO}_{3.9}$. Orange, purple and pale blue dots represent ions originally on O1, O2 and Co sites respectively. La and Sr ions in between layers have been omitted for the sake of clarity.

we find oxide-ion migration between two apical positions (O2) belonging to adjacent perovskite layers (box X in Fig. 7); in the second case, oxide ion migration involves equatorial (O1) and apical (O2) positions within a CoO_6 octahedron.

We note that Fig. SI-3 (ESI[†]) shows, as an example, the mean square displacement (MSD) parameters as a function of time for $\text{La}_{0.8}\text{Sr}_{1.2}\text{CoO}_{3.9}$ at 1773 K and indicates that, as predicted, O1 moves faster than O2 while the cations vibrate around their lattice positions. Oxygen diffusion coefficients (*D*) in the temperature range 1173–1973 K were derived from the slope of the mean square displacement (MSD) parameters *vs.* time plots; the mean values of MSD for O1 and O2 have been used since the analysis of the scatter plots and of the MSD *vs.* time plots reveals a simultaneous participation of both species. Calculated oxygen diffusion coefficients are in the range 10^{-8} to 10^{-7} $\text{cm}^2 \text{s}^{-1}$ (Fig. 8). There are no experimental values for these specific compositions to allow direct comparison, although the calculated range is consistent with the experimental diffusion coefficients derived for the related undoped La_2NiO_4 and La_2CoO_4 materials.^{8,25} The calculated activation energy derived from the MD simulations is 0.76 eV. The trend in the activation energies for oxygen vacancy migration reported in Table 2 is consistent with the results reported for the lanthanum nickelate system,^{11,13} although the results obtained from MD simulations show a better quantitative agreement.

The experimental indication is that activation energies for oxide ion diffusion in the $\text{La}_2\text{Ni}_{1-x}\text{Co}_x\text{O}_{4+\delta}$ system decrease as the Co content increases,²⁵ which is reproduced by previous simulation studies of $\text{La}_2\text{NiO}_{4+\delta}$ and $\text{La}_2\text{CoO}_{4+\delta}$,^{11,12} where the mobile species is interstitial oxygen. We recall here that, in contrast to previous studies, our calculations have been performed on heavily doped samples in the $\text{La}_{2-x}\text{Sr}_x\text{CoO}_4$ system. The difference in the nominal oxidation state of Co and the presence of a large number of Sr ions might influence the absolute values of the defects involved, even though the trends are preserved. In particular, possible defect association and vacancies ordering may lead to a reduction in conductivity and an increase in activation energy, as suggested for other perovskite systems.^{30,31} We have therefore calculated the binding energies for the formation of neutral clusters in LaSrCoO_4 of

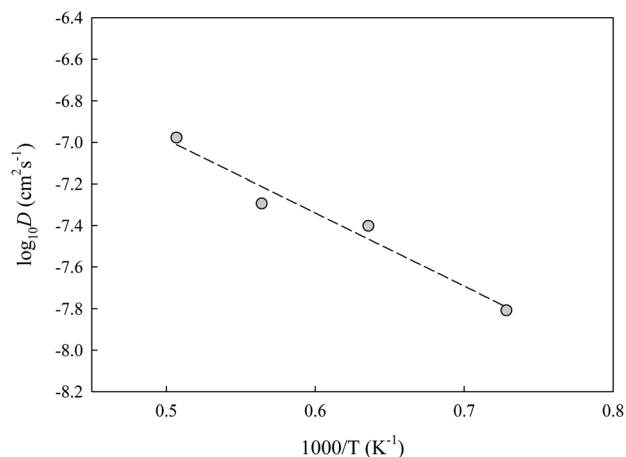


Fig. 8 Arrhenius plot of the calculated oxygen diffusion coefficient for $\text{La}_{0.8}\text{Sr}_{1.2}\text{CoO}_{3.9}$.

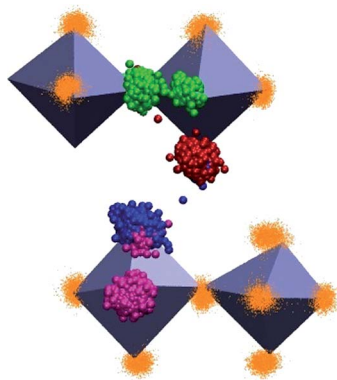


Fig. 9 3D representation of the event highlighted in box X of Fig. 7a, showing oxygen migration between equatorial and apical positions within a CoO_6 octahedron (pink and red), between equatorial and equatorial positions (green) and between apical positions belonging to separate layers (blue). La and Sr ions have been omitted for clarity. Each oxygen involved in the migration event is represented by a different colour; spheres of the same colour indicate the positions occupied by a specific atom over the simulation time.

configurations $\text{Sr}_{\text{La}'} - \text{V}_{\text{O}}'' - \text{Sr}_{\text{La}'}$ and $\text{La}_{\text{Sr}'} - \text{O}_{\text{int}}'' - \text{La}_{\text{Sr}'}$. The estimated binding energies are -0.33 and -0.14 eV per defect, respectively, which suggests that formation of neutral clusters in this system is indeed favoured, and warrant further investigation.

Fig. 9 is a 3D representation of the migration paths presented in Fig. 7a, where each oxygen involved is indicated with a different colour. This clearly shows the three migration paths with lowest activation energies for vacancy migration in the oxygen-deficient $\text{LaSrCoO}_{4-\delta}$ -based material, as derived by energy minimization techniques (Table 2). In particular, these are (i) vacancy migration between equatorial positions and equatorial-apical positions along the edges of the octahedron and (ii) vacancy migration between apical positions of CoO_6 octahedra belonging to adjacent perovskite layers along the c -axis.

In summary, analysis of the MD results suggests that oxide ion migration in the ab plane is favoured in oxygen sub-stoichiometric samples, as predicted for undoped La_2NiO_4 and La_2CuO_4 ,^{13,16,32} but vacancy migration is not necessarily restricted to the perovskite layer, since jumps do occur between apical oxygens of adjacent layers.

3.3 Oxygen-excess material: interstitial migration

Oxygen interstitial migration in Ni-based K_2NiF_4 -type oxides such as $\text{La}_2\text{NiO}_{4+\delta}$ has been extensively investigated by modelling techniques, and it has been shown to proceed mainly through an interstitialcy mechanism restricted to the ab plane.¹⁴ The migration path involves the O2 site (apical position) and the oxygen interstitial site.

For completeness, we have also considered the mechanistic details on oxygen interstitial migration in heavily doped $\text{La}_{2-x}\text{Sr}_x\text{CoO}_4$ and oxygen-rich materials for the first time. Indeed, the results of this MD study confirm the presence of an analogous migration path and interstitialcy mechanism for the $\text{La}_{1.2}\text{Sr}_{0.8}\text{CoO}_{4.1}$ composition.

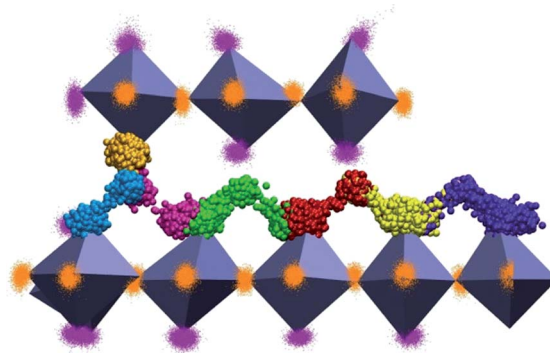


Fig. 10 3D representation of oxygen interstitial migration in $\text{La}_{1.2}\text{Sr}_{0.8}\text{CoO}_{4.1}$. La and Sr ions have been omitted for clarity. Each oxygen involved in the migration event is represented by a different color. Spheres of the same color indicate the positions occupied by a specific atom over the simulation time.

Fig. 10 shows a 3D representation of long-range interstitial migration as derived by MD simulations for $\text{La}_{1.2}\text{Sr}_{0.8}\text{CoO}_{4.1}$; the participation of the O2 apical oxygens in the diffusion process is shown, whereas the O1 equatorial positions are not involved.

Oxygen diffusion is therefore highly anisotropic and restricted to the ab plane, in between the perovskite layers. Fig. 10 clearly shows the typical “wave-like” migration path observed for interstitial migration in K_2NiF_4 -type oxides from recent modelling studies,^{9,11,14} as well from structural studies of Pr_2NiO_4 based materials using maximum entropy methods.^{6,7} Fig. SI-2 (ESI†) shows the mean square displacements (MSD) for $\text{La}_{1.2}\text{Sr}_{0.8}\text{CoO}_{4.1}$ which confirm that the most mobile species are the O2 apical oxygen and the interstitial oxygen.

For the calculations of the diffusion coefficients, the mean values of MSD for O2 and O3 have been used, since the analysis of the scatter plots and of the MSD vs. time plots reveals a simultaneous participation of both species. The calculated oxygen diffusion coefficients are slightly higher than the vacancy diffusion coefficients (Fig. 11), with a similar activation energy of 0.71 eV.

Finally, it is interesting to note that Fig. 10 also shows that the migrating oxide-ions have a relatively long residence time at

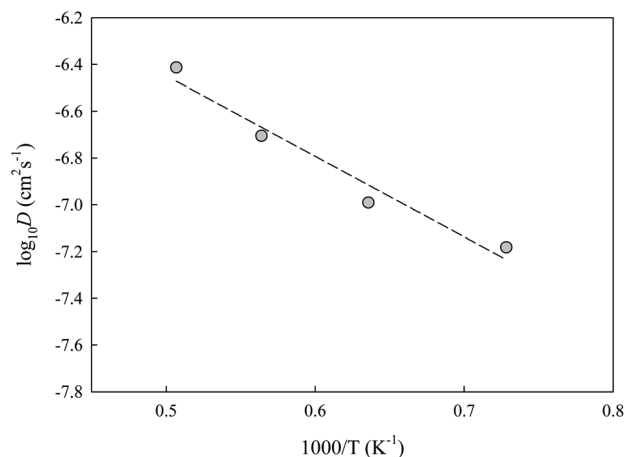


Fig. 11 Arrhenius plot of the calculated oxygen diffusion coefficient for $\text{La}_{1.2}\text{Sr}_{0.8}\text{CoO}_{4.1}$. The line is a guide for the eyes only.

the O2 apical position. The region of occupied space around the starting O2 position during the MD simulation is in agreement with the shape and size of the thermal ellipsoids found from neutron diffraction data on related systems.⁶ As indicated previously,¹⁴ this accounts for the tilting of the CoO₆ octahedra, which assists oxygen migration through the interstitialcy mechanism in this K₂NiF₄-type structure.

4. Conclusions

A powerful combination of energy minimization and MD techniques has been used to investigate oxide ion migration mechanisms in the heavily doped K₂NiF₄-type system, La_{2-x}Sr_xCoO_{4±δ}. This class of compounds is receiving considerable attention as potential cathode materials for intermediate temperature solid oxide fuel cells (IT-SOFCs). However, the majority of previous work has focused on oxygen over-stoichiometric samples with no acceptor doping, in which oxide ion migration is mediated only by interstitial oxygen. Here, we present results on the La_{2-x}Sr_xCoO_{4±δ} system with a high level of doping ($x > 0.8$), where both oxygen vacancy and interstitial conduction mechanisms are considered.

Firstly, the results of this study support the hypothesis of favourable migration of oxygen vacancies within the perovskite layer of the structure, but also indicate possible long-range paths between adjacent layers for vacancy conduction; this is of general significance to related acceptor-doped and oxygen-deficient oxides based on LnSrMO₄ (where Ln = La, Nd, Pr; M = Co, Ni, Cu). Secondly, interstitial oxygen conduction in oxygen hyperstoichiometric compositions is *via* an interstitialcy mechanism and along a 'wave-like' 2D path between apical and interstitial sites within the *ab* plane, as found for related K₂NiF₄ type compounds. Owing to the lack of experimental data on oxygen vacancy diffusion in heavily doped La_{2-x}Sr_xCoO_{4±δ} it is hoped that our study will stimulate further investigations in this area.

Acknowledgements

Financial support from the Cariplo Foundation is gratefully acknowledged.

Notes and references

1 J. B. Goodenough, *Rep. Prog. Phys.*, 2004, **67**, 1915.

- 2 A. Tarancon, M. Burriel, J. Santiso, S. J. Skinner and J. A. Kilner, *J. Mater. Chem.*, 2010, **20**, 3799.
- 3 L. Malavasi, C. A. J. Fisher and M. S. Islam, *Chem. Soc. Rev.*, 2010, **39**, 4370.
- 4 S. J. Skinner, *Solid State Sci.*, 2003, **5**, 419.
- 5 F. Riza and Ch. Ftikos, *J. Eur. Ceram. Soc.*, 2007, **27**, 571.
- 6 M. Yashima, N. Sirikanda and T. Ishihara, *J. Am. Chem. Soc.*, 2010, **132**, 2385.
- 7 M. Yashima, M. Enoki, T. Wakita, R. Ali, Y. Matsushita, F. Izumi and T. Ishihara, *J. Am. Chem. Soc.*, 2008, **130**, 2762.
- 8 S. J. Skinner and J. A. Kilner, *Solid State Ionics*, 2000, **135**, 709.
- 9 M. S. D. Read, M. S. Islam, F. E. Hancock and F. King, *J. Phys. Chem. B*, 1999, **103**, 1558.
- 10 M. S. D. Read, M. S. Islam, G. W. Watson and F. E. Hancock, *J. Mater. Chem.*, 2001, **11**, 2597.
- 11 A. Chroneos, D. Parfitt, J. A. Kilner and R. W. Grimes, *J. Mater. Chem.*, 2010, **20**, 266.
- 12 D. Parfitt, A. Chroneos, J. A. Kilner and R. W. Grimes, *Phys. Chem. Chem. Phys.*, 2010, **12**, 6834.
- 13 A. R. Cleave, J. A. Kilner, S. J. Skinner, S. T. Murphy and R. W. Grimes, *Solid State Ionics*, 2008, **179**, 823.
- 14 A. Kushima, D. Parfitt, A. Chroneos, B. Yildiz, J. A. Kilner and R. W. Grimes, *Phys. Chem. Chem. Phys.*, 2011, **13**, 2242.
- 15 V. Vashook, H. Ullmann, O. P. Olshevskaya, V. P. Kulik, M. E. Lukashevich and L. V. Kochanovskij, *Solid State Ionics*, 2000, **138**, 99.
- 16 N. L. Allan and W. C. Mackrodt, *Philos. Mag. A*, 1991, **64**, 1129.
- 17 C. Tealdi, C. Ferrara, L. Malavasi, P. Mustarelli, C. Ritter, G. Chiodelli and Y. A. Diaz-Fernandez, *Phys. Rev. B: Condens. Matter Mater. Phys.*, 2010, **82**, 174118.
- 18 T. Matsuura, J. Tabuchi, J. Mizusaki, S. Yamauchi and K. Fueki, *J. Phys. Chem. Solids*, 1988, **49**, 1403.
- 19 J. D. Gale, *J. Chem. Soc., Faraday Trans.*, 1997, **93**, 629.
- 20 B. G. Dick and A. W. Overhauser, *Phys. Rev.*, 1958, **112**, 90.
- 21 N. F. Mott and M. J. Littleton, *Trans. Faraday Soc.*, 1938, **34**, 485.
- 22 W. Smith and T. R. Forester, *J. Mol. Graphics*, 1996, **14**, 136.
- 23 W. Humphrey, A. Dalke and K. Schulten, *J. Mol. Graphics*, 1996, **14**, 33.
- 24 L. Minervini, R. W. Grimes, J. A. Kilner and K. E. Sickafus, *J. Mater. Chem.*, 2000, **10**, 2349.
- 25 C. N. Munnings, S. J. Skinner, G. Amow, P. S. Whitfield and I. J. Davidson, *Solid State Ionics*, 2005, **176**, 1895.
- 26 M. S. Islam, *Solid State Ionics*, 2002, **154–155**, 75.
- 27 C. Tealdi, L. Malavasi, C. A. J. Fisher and M. S. Islam, *J. Phys. Chem. B*, 2006, **110**, 5395.
- 28 C. Tealdi, P. Mustarelli and M. S. Islam, *Adv. Funct. Mater.*, 2010, **20**, 3874.
- 29 E. Kendrick, J. Kendrick, K. S. Knight, M. S. Islam and P. R. Slater, *Nat. Mater.*, 2007, **6**, 871.
- 30 M. Cherry, M. S. Islam and C. R. A. Catlow, *J. Solid State Chem.*, 1995, **118**, 125.
- 31 C. A. J. Fisher, *et al.*, *J. Eur. Ceram. Soc.*, 2005, **25**, 3243.
- 32 S. N. Savvin, G. N. Mazo and A. K. Ivanov-Schitz, *Crystallogr. Rep.*, 2008, **53**, 291.